Article

Study of the Interaction of Sorption and Catalytic Centers in Carboxypeptidase T by X-ray Analysis

Valerij Akparov [1,*](#)[ID], Vladimir Timofeev [2], Inna Kuranova [2] and Ilias Khaliullin [3]

1 Protein Chemistry Department, NRC "Kurchatov Institute", Akademika Kurchatova pl. 1, 123182 Moscow, Russia
2 Shubnikov Institute of Crystallography of Federal Scientific Research Centre "Crystallography and Photonics" Russian Academy of Sciences, Leninskii Prospect 59, 119333 Moscow, Russia; tostars@mail.ru (V.T.); inna@crys.ras.ru (I.K.)
3 Moscow Institute of Physics and Technology, National Research University, 9 Institutskiy per., Dolgoprudny, 141701 Moscow, Russia; khig@mail.ru
* Correspondence: valery.akparov@yandex.ru

Abstract: Carboxypeptidase T (CPT; EC 3.4.17.18) from *Thermoactinomyces vulgaris* is a distant homolog of the highly specific pancreatic carboxypeptidase B; but has a broad substrate specificity; the source of which remains unclear. A previous study of the structural bases of the substrate specificity of CPT using stable sulfamoyl analogs of the transition state of the elimination of leucine; phenylalanine; arginine; and glutamic acid; showed that the binding of the C-terminal residue of the substrate to the primary selectivity pocket of CPT leads to a change in the distance between Zn^{2+} and the sulfur atom. This value is related to the efficiency of catalysis of the corresponding substrate or the inhibition constant of the corresponding stable analog of the transition state. In this work; we obtained crystallographic and kinetic data of the complex of CPT with N-sulfamoyl-L-valine; confirming the effect of the binding of the ligand's side group by the primary specificity pocket of CPT on the structure of the catalytic center; which can explain the unusual substrate specificity of CPT.

Keywords: carboxypeptidase T; transition-state complex; X-ray analysis; S1'-site- catalytic site interaction; N-sulfamoyl-L-valine

1. Introduction

Metallocarboxypeptidases (MCPs) are zinc-dependent hydrolases. Increasing attention to them is caused by their involvement in important physiological processes such as food digestion, neuropeptide processing, blood clotting, inflammation, and carcinogenesis [1–3]. MCPs are used in biotechnology such as insulin production. In this regard, there is an interest in the rational redesign of MCPs to improve their activity, thermal stability, and substrate specificity. The successful enzyme design is based on a correct understanding of the substrate recognition mechanism.

Thanks to the works of Vallee, Lipscomb, and others [4–6], metallocarboxypeptidase A (MCPA) is probably the most studied enzyme. Back in the 60 s of the last century, the crystal structure was found, and the substrate recognition mechanism was exposed, in which the primary specificity pocket or S1'-subsite according to the Schechter and Bergman nomenclature plays the main role [7]. The residue at the bottom of the primary specificity pocket is considered to be crucial for binding. In hydrophobic selective CPA, it is an isoleucine residue 255, while in positively charged selective carboxypeptidase B (CPB), it is negatively charged aspartic acid residue 255. In carboxypeptidase O (CPO) at the bottom of the pocket of primary specificity, there is an arginine residue 275 [8], and CPO selectively cleaves off negatively charged residues. The role of the residual at the bottom of the pocket of the primary specificity of metallocarboxypeptidases (MCP) was confirmed by the results

of mutagenesis of Asp255Arg [9], Arg275Asp, Arg275Ala [10], that converted CPB to CPO, CPO to CPB, and CPA, which are similar enzymes.

Carboxypeptidase T (CPT, EC 3.4.17.18) from the thermophilic microorganism *Thermoactinomyces vulgaris* is a distant homolog of pancreatic CPA and CPB, but it has the same type of three-dimensional structure, identical catalytic center, and a sorption center similar in structure to CPB [11]. At the bottom of the binding pocket of the primary specificity of CPT, there is an aspartic acid residue 260. Nevertheless, CPT doesn't show only similar to CPB specificity towards positively charged residues, but in contrast to CPB, has a wide substrate specificity [12] and is able to cleave both (predominantly) hydrophobic and positively or negatively [13] charged residues from the C-termini of peptide substrates.

Moreover, the complete replacement of all the residues of the primary specificity pocket of CPT with the corresponding CPB residues didn't shift the selectivity of CPT towards CPB [14]. This suggests that the specificity of CPT is provided in a different way than the simple hydrophobic and charge complementarity of the primary specificity pocket and the side group of the C-terminal residue of the substrate.

CPB has a "rigid" structure, and upon binding of such different substrates as phenylalanine or arginine-containing substrates, the structure of the transition complex remains unchanged [15]. The substrate selectivity of CPB is implemented by the type of conformational selection. In the case of CPT, the position of the substrate's side chain in the enzyme-substrate complex may change (V.Akparov et al., 2015). The structure of the tetrahedral transition complex also changes from one substrate to another [16]. In this case, the recognition of the substrate is carried out according to the principle of induced fit. This conclusion was made on four analogs of the transition state, sulfamoyl derivatives of phenylalanine, leucine, arginine, and glutamic acid.

In this work, at microgravity conditions on the ISS, we crystallized the CPT complex with N-sulfamoyl-L-valine, which has the symmetry of the spatial group P6322, then obtained crystallographic and kinetic data of the CPT complex, and studied the effect of the lateral group of the valine inhibitor on the interatomic distances in the transition complex.

It is well-known that carboxypeptidases have different kinds of active centers, with and without catalytic metal ions (serine carboxypeptidases) or with one or two catalytic metal ions. This ion can be replaced with cadmium, cobalt (Insight into the transition between the open and closed conformations of Thermus thermophilus carboxypeptidase. Ref. [17], nickel ions. The influence of calcium ions on substrate selectivity of carboxypeptidase T was a subject of one of our previous works. In this paper, the dependence of the geometry of the coordination sphere of the zinc ion on the nature of the substrate is clarified.

2. Materials and Methods

Subtilisin 72 [18], peptide substrates ZAAL-pNA (N-benzyloxycarbonyl-alanyl-alanyl-leucine-nitroanilide) [19], ZAAL (N-benzyloxycarbonyl-alanyl-alanyl-leucine) [20] were prepared in our laboratory. Affinity sorbent ([N-(ε-amino-caproyl)-p-aminobenzyl]succinyl-Sepharose 4B (CABSSepharose) was prepared according to previously described protocols [21]. Ultrafiltration cells and PM10 membranes were from Amicon (Millipore-Sigma, Birlington, MA, USA), glass capillaries 60-mm in length, and inner diameter of 0.5 mm for CPT crystallization from Confocal Science Inc., (Tokyo, Japan). Deionized water MilliQ (MilliporeSigma, Burlington, MA, USA) with a resistance of 19 MOhm/cm, 2-methyl-2,4-pentadiol (MPD), L-cystine and L-cysteine, diisopropylfluorophosphate, isopropyl-β-D-thiogalactoside (IPTG), 3-[(3-cholamidopropyl)dimethylammonio]-1-propanesulfonate (CHAPS), and 4-morpholinoethansulfonic acid (MES), and porcine carboxypeptidase B were obtained from Sigma-Aldrich (St. Louis, MO, USA). The kinetic experiments were performed in the thermostated cell of the PC-connected Shimadzu UV-1800 spectrophotometer (Shimadzu, Kyoto, Japan).

2.1. Macromolecule Production

The gene encoding pro-CPT was cloned into a pET23a vector [22]. After transformation in BL21(DE3) pLysS cells (Novagen, EMB Bioscience Inc., San Diego, CA, USA), the cells were reseeded in test tubes containing 5 mL of LB medium with 120 mg L^{-1} ampicillin and 34 mg L^{-1} chloramphenicol and incubated for 18 h at 301 K. The cells were then reseeded in flasks containing the same medium with added IPTG (1 mM) and incubated for a further 6 h at 301 K. The cells were expressed and then lysed by sonication. The inclusion bodies were separated from the cell lysate by centrifugation (20,000 rpm× g, 20 min), washed with 0.05% CHAPS (*w/v*), 2 M NaCl, and water, and dissolved in 8 M urea to obtain a final protein concentration of 5 gL^{-1}. Then, 100 mL of the protein solution was added dropwise with vigorous stirring into 1 L of 50 mM Tris/HCl pH 8.0 containing 30% glycerol (*v/v*), 0.5 M NaCl, and 10 mM $CaCl_2$. The solution was incubated for 16 h at 310 K. After incubation, the solution was further diluted two-fold with 50 mM Tris/HCl pH 8.0, 0.5 M NaCl, and 10 mM $CaCl_2$ and concentrated to a volume of 20 mL by ultrafiltration. Pro-CPT was activated by incubation with subtilisin 72 (molar ratio of CPT: subtilisin was 1:200) for 4 h at 310 K. The reaction was stopped with diisopropylfluorophosphate. The protein solution was concentrated to a volume of 0.5 mL, and the pH was adjusted to 6.0 using 100 mM MES pH 5.8. The protein solution was then purified using a CABS Sepharose column [21] (20 mL) equilibrated with 10 mM MES pH 6.0 containing 0.5 M NaCl, 10 mM $CaCl_2$, and 0.1 mM ZnSO4. CPT was eluted with the same buffer at pH 8.0, and CPT-containing fractions were pooled. The buffer was replaced by the crystallization buffer (0.01 M MES/NaOH pH 6.0 containing 1 mM $CaCl_2$, 0.1 mM $ZnSO_4$, and 0.25 M NaCl). Finally, the protein was concentrated to 10 gL^{-1} and sterile filtered using 0.22 μm Ultrafree-CL LG Centrifugal Filter (Merck).

2.2. Crystallization

Crystals of CPT in the complex with SVal were grown in microgravity using the counter-diffusion technique. The equipment and technology developed by the Aerospace Agency of Japan JAXA were used for crystal growth as per previously described methods [23,24]. A glass capillary (0.5 mm in diameter) filled with the protein-containing solution served as a crystallization device. One end of the capillary was hermetically sealed while the other end was connected to a silicon pipe (0.5 mm) filled with 1% agarose gel and plunged into a cylinder containing the precipitating solution. All six cylinders with capillaries were placed in a polyethylene case containing a small amount of water. The cases were hermetically sealed and placed in containers. The containers were delivered to the space launching center in a thermal insulated bag [25,26]. The present crystallization setup was chosen because the slow diffusion of precipitant into protein solution through a gel layer under zero gravity conditions improves the diffraction properties of protein crystals [27]. For data collection, the crystals were extracted from the capillary, placed in a precipitant solution with 20% glycerol (*v/v*) as a cryoprotectant, and flash-cooled in a nitrogen vapor flow. The crystallization process has been summarized in Table 1.

Table 1. Crystallization.

Method	Counter-Diffusion Technique (in Microgravity)
Capillary type	Glass capillary
Temperature (K)	293
Protein concentration (gL^{-1})	10
Protein-containing solution (capillary)	10 mM MES buffer pH 6.0, 0.25 M NaCl, 0.1 mM $ZnSO_4$ and 1 mM $CaCl_2$
Precipitating solution (cylinder)	1.4 M $(NH_4)2SO_4$, 50 mM MES pH 6.0, 0.1 mM $ZnSO_4$, 1 mM $CaCl_2$, 5% MPD, and 100 mM N-sulfamoyl-L-Valine

2.3. Data Collection and Processing

Diffraction data from the crystal was collected by the rotation method using iMosflm software [28] to process the experimental intensities. The diffraction data reported in Table 2 were obtained from a single crystal.

Table 2. Data collection and processing.

Diffraction Source	Spring8 Beamline BL41XU
Wavelength (Å)	0.8
Temperature (K)	100
Detector	DECTRIS EIGER X 16M
Crystal-detector distance (mm)	300
Rotation range per image (°)	0.1
Total rotation range (°)	360
Exposure time per image (s)	0.1
Space group	P6322
a, b, c (Å)	157.531, 157.531, 104,523
α, β, γ (°)	90, 90, 120
Mosaicity (°)	0.11
Resolution range (Å)	30.00–1.9 (2.0–1.9)
No. of unique reflections	60,407
Completeness (%)	99.97 (99.89)
Redundancy	17.49 (18.25)
$\langle I/\sigma(I)\rangle$	7.7316 (2.16)
Rmerge	0.144 (0.330)

Values for the outer shell are given in parentheses.

2.4. Structure Solution and Refinement

The structure of the CPT complex with SVal was determined at 1.9 Å resolution by the molecular-replacement method using Phaser [29] with the atomic coordinates of CPT (PDB entry:3QNV) as a starting model. For anisotropic structure refinement, REFMAC [30] was used. Manual correction of the models was performed using Coot [31], and electron-density maps were calculated with $2|Fo|-|Fc|$ and $|Fo|-|Fc|$ coefficients. Water molecules and calcium ions were located in the electron-density maps, and difference Fourier synthesis revealed electron density in the active site which was identified as a ligand. The ligand was refined with an occupancy of 100%. The coordinates of the structure have been deposited in the PDB (PDB entry: 6TNK). The refinement statistics are presented in Table 3. Pymol (Schrödinger LLC, 2015) software was used for making Figure 1.

2.5. Kinetic Experiments

All the kinetic experiments were carried out at 298 K in 0.25 M Tris-HCl buffer with 0.01 M $CaCl_2$ and pH 7.5. Tripeptide substrate N-(benzyloxycarbonyl)-Ala-Ala-Val-OH (ZAAV) in proper concentrations was used. Enzymatic reactions were followed by using PC connected Shimadzu UV-1800 spectrophotometer at 225 nm. Reaction mixtures were prepared in a 500 mL quartz cuvette with an optical path length of 1 cm. Then a small amount of enzyme was added to the reaction mixture to start the reaction.

Kinetic parameters of substrates conversion were determined using the initial rates method. Initial rates of the enzymatic reactions were obtained for different substrate concentrations in the range of 0.1–2 mM. Then "substrate concentration—reaction rate" data points were fitted to the Michaelis-Menten equation using SciDAVis software.

Inhibitors' binding constants were determined using the integral kinetics method. Progress curves of the specific substrate N-(benzyloxycarbonyl)-Ala-Ala-Leu-OH (ZAAL) conversion were registered in the presence of different concentrations of inhibitor and then linearized as described earlier [16] to obtain apparent KM over Vmax values (KMapp/Vmax). Then "inhibitor concentration—KMapp/Vmax" data points were later fitted to the linear equations y = ax + b, from which inhibition constants were calculated as b/a.

Table 3. Structure refinement.

Resolution Range (Å)	20–1.9 (1.95–1.9)
Completeness (%)	99.9 (99.8)
σ cutoff	F > 0.000σ(F)
No. of reflections, working set	57327 (4173)
No. of reflections, test set	3001 (193)
Final Rcryst	0.142 (0.156)
Final Rfree	0.151 (0.168)
No. of non-H atoms	
Protein	2581
Ion	6
Ligand	12
Water	262
R.m.s. deviations	
Bonds (Å)	0.014
Angles (°)	1.845
Average B factor (Å2)	13.76
Ramachandran plot	
Favoured regions (%)	98.0
Additionally allowed (%)	2.0
Outliers (%)	0.0

Values for the outer shell are given in parentheses.
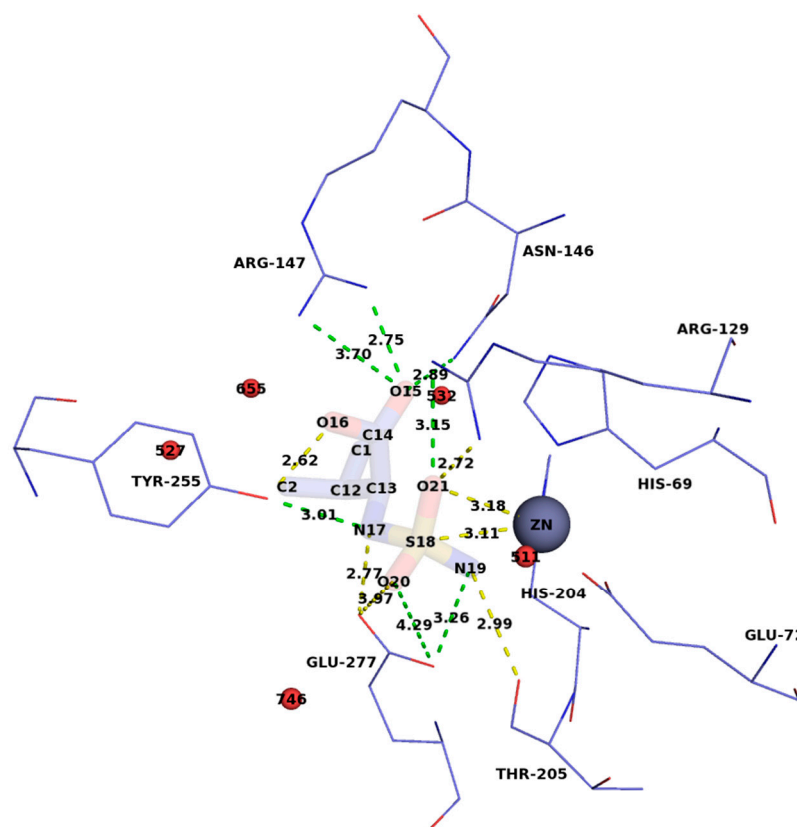
Figure 1. Location of SVal in the active center of CPT. S–Zn^{2+} and O–Zn^{2+} gaps and hydrogen bonds are indicated in yellow, the lengths of which are proportional to the logarithms of the association constants (lg(1/Ki) and the catalysis efficiencies lg (kcat/Km)). Other hydrogen bonds and interatomic distances are shown in green, water molecules in red.

3. Results and Discussion

The final model of the CPT-SVal complex was refined to a resolution of 1.92 Å (Rfree = 0.161). The asymmetric block contained one protein molecule (molecule A, residues

1–323), one zinc ion per protein molecule, and 269 water molecules. The CPT polypeptide chain was complete and clearly traced on the electron density map (Asp1-Cys323), the active center of the enzyme contained electron density, which was interpreted as SVal molecule (Figure S1).

The SVal molecule was linked with catalytic zinc ion by a 2.0 Å length N2—Zn bond, SVal atom naming scheme is shown in Figure 1.

The sulfamoyl part of SVal had a tetrahedral configuration that simulated sp^3-hybridized C-atom configuration in a complex with the substrate. The sulfamoyl binding mode was similar to those found in previously reported CPA—SPhe (PDB ID: 1IY7 [32] and CPT– SLeu (PDB ID: 6GO2 [16]) complexes. The SVal side chain was anchored in the S1′-subsite, which is the pocket of the primary substrate specificity of the CPT. The environment of the SVal molecule in the active site of CPT is shown in Figure 1. Glu277 acts as a general base catalyst that deprotonates water molecule (O20), and Zn ion activate carbonyl oxygen imitated by N19. Arg129 and Tyr255 participate in the stabilization of transition-state by bonding with an oxygen atom (O21 in sulfamoyl analog) and nitrogen (N17 in SVal) corresponding.

We have previously shown [16] that the geometry of the transition complex analog formed upon binding of the sulfamoyl transition state analog to the active center of CPT depends on the nature of the side group of the sulfamoyl inhibitor. It is expressed in the fact that the length of the connections between the ligand atoms and the catalytic center groups in enzyme complexes changes as one ligand switched for another. At the same time, the logarithms of the inhibitors association constants and the logarithms of the catalysis efficiency constants (k_{cat}/K_M) of the corresponding tripeptide substrates change the same way (see the figures).

Earlier, such a correlation between bond lengths and inhibition constants/catalysis efficiency constants were obtained for SLeu, SPhe, SArg, and SGlu inhibitors and O21-R129NH1, O21-Zn^{2+}, N19-T205 (O), S-Zn^{2+}, N17-E277OE2, O16-Y255OH bonds. Though, the Ka value can both increase and decrease with increasing bond lengths.

In this work, we show that the same is also relevant for the sulfamoyl analog of the transition state of valine substrate conversion. The inhibition constant of N-sulfamoylvaline is higher than Ki for the hydrophobic leucine and phenylalanine analogs, but less than the inhibition constant of charged inhibitors—arginine and glutamic acid analogs. The above bond lengths for N-sulfamoylvaline are between the corresponding SLeu and SArg bond lengths.

The same correspondence (ln(kcat/Km) = kΔl, where Δl is the bond length, kcat/Km is the effectiveness of catalysis and k is the proportionality coefficient) is observed between the logarithm of the catalysis efficiency of tripeptide substrates conversion and the bond length between the ligand atoms and catalytic residues. In this case, the constant of inhibition of CPT by the SVal analog of the transition state exceeds the corresponding constants for SPhe and SLeu but is less than the constant for SArg.

The coordination sphere of the catalytic zinc ion is also involved in catalysis and its dependence on the nature of the side groups of the substrate is determined for it. This dependence does not look as bright as in the case of a tetrahedral transition complex, however, in three out of four cases, the distances of Zn^{2+}—His204ND1, Zn^{2+}—Glu72OE2, Zn^{2+}—Glu72OE1 in complex with SGlu differ significantly from the same distances in complexes with hydrophobic inhibitors, including SVal (see Figure 2 and Supplementary Materials). In this respect, the zinc complex with its ligands is similar to the complex of a sulfonyl group with a catalytic center. An increase in the resolution of X-ray diffraction analysis can clarify the role of the coordination distances of zinc in the induced correspondence in the recognition of the substrate.
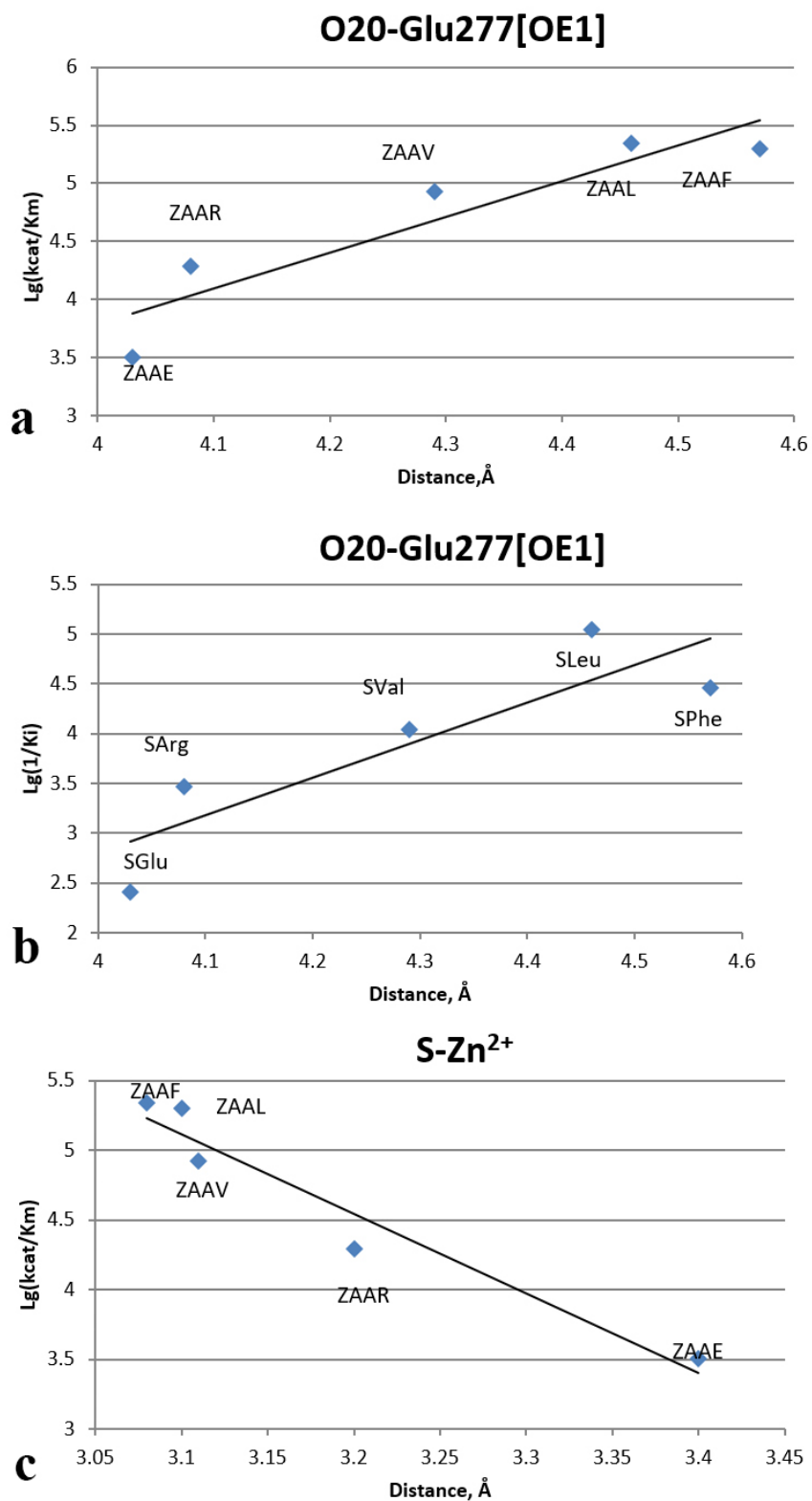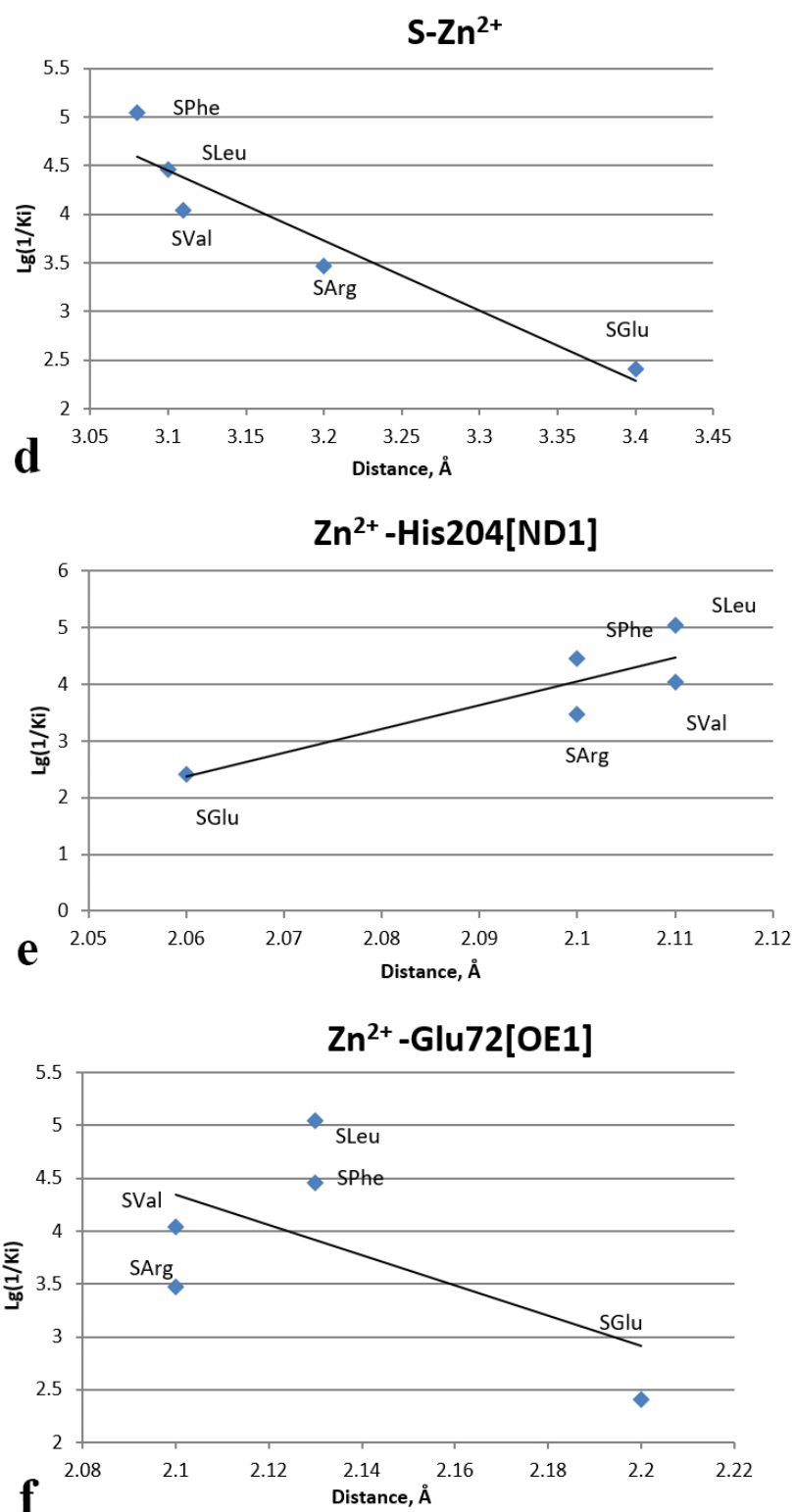
Figure 2. *Cont.*

Figure 2. Dependence of Lg(1/Ki) (**a**), Lg(kcat/Km) (**b**) on the O20-E277[OE1] distances in a line of CPT substrates and inhibitors; Lg(kcat/Km) (**c**) and Lg(1/Ki) (**d**) on the S-Zn^{++} distances in a line of CPT substrates and inhibitors; Lg(1/Ki) (**e**) on the Zn^{2+} -His204ND1 and Lg(1/Ki) (**f**) on the Zn^{2+} -Glu72OE1 distances in a line of CPT substrates and inhibitors: N-sulfamoyl-Glutamic acid, SGlu; N-sulfamoyl-Arginine, SArg; N-sulfamoyl-Valine, SVal; N-sulfamoyl-Leucine, SLeu; N-sulfamoyl-Phenylalanine, SPhe. Substrates are represented in one-letter code, Z = carbobenzoxy.

4. Conclusions

The crystal structure of the complex of the sulfamoyl analog of valine and microbial carboxypeptidase T is obtained. Comparison of intermolecular distances and kinetic constants for this complex shows that the broad substrate specificity of carboxypeptidase T is determined to a large extent not by the complementarity of the side group of the ligand S1′-subsite, but by the distortion of the structure of the tetrahedral transition complex, and this distortion depends on the size of the side group of the ligand, and the efficiency of cleavage of valine is between the efficiency of cleavage of leucine and arginine. The distances inside the coordination sphere of the zinc atom also change during the transition from one CBT complex to another. This is a new example of the participation of induced compliance in the selectivity of enzymes, demonstrating the influence of the structure of the side groups of the substrate on the catalytic activity of the enzyme.

Supplementary Materials: The following are available online at https://www.mdpi.com/article/10.3390/cryst11091088/s1, Figure S1: Electron density for SVal. The ligand omitted Fo-Fc map is contoured at 2 r.m.s.d. The atoms colors are carbon (green), nitrogen (blue), oxygen (red), sulfur (yellow). Atom numbering for SVal is shown.

Author Contributions: Conceptualization, V.A.; methodology, V.A., V.T., I.K. (Inna Kuranova) and I.K. (Ilias Khaliullin); software, V.T.; validation, V.T.; formal analysis, V.A.; investigation, V.A., V.T., I.K. (Inna Kuranova) and I.K. (Ilias Khaliullin); resources, V.A. and I.K. (Inna Kuranova); data curation, V.T. and V.T.; writing—original draft preparation, V.A.; writing—review and editing, V.A. and I.K (Ilias Khaliullin).; visualization, V.T.; supervision, V.A.; project administration, V.A.; funding acquisition, V.A. and I.K (Inna Kuranova). All authors have read and agreed to the published version of the manuscript.

Conflicts of Interest: The authors declare no conflict of interest.

References

1. Turk, B.; Turk, D.; Turk, V. Protease signalling: The cutting edge. *EMBO J.* **2012**, *31*, 1630–1643. [CrossRef]
2. Pérez-Silva, J.G.; Español, Y.; Velasco, G.; Quesada, V. The Degradome database: Expanding roles of mammalian proteases in life and disease. *Nucleic Acids Res.* **2016**, *44*, D351–D355. [CrossRef] [PubMed]
3. Bunnage, M.E.; Blagg, J.; Steele, J.; Owen, D.R.; Allerton, C.; McElroy, A.B.; Miller, D.; Ringer, T.; Butcher, K.; Beaumont, K.; et al. Discovery of potent & selective inhibitors of activated thrombin-activatable fibrinolysis inhibitor for the treatment of thrombosis. *J. Med. Chem.* **2007**, *50*, 6095–6103.
4. Vallee, B.L.; Neurath, H. Carboxypeptidase, a zinc metalloenzyme. *J. Biol. Chem.* **1955**, *217*, 253–262. [CrossRef]
5. Christianson, D.W.; Lipscomb, W.N. Carboxypeptidase A. *Acc. Chem. Res.* **1989**, *22*, 62–69. [CrossRef]
6. Lipscomb, W.M.; Strater, N. Recent Advances in Zinc Enzymology. *Chem. Rev.* **1996**, *96*, 2375–2433. [CrossRef]
7. Schechter, I.; Berger, A. On the size of the active site in proteases. I. Papain. 1967. *Biochem. Biophys Res. Commun.* **2012**, *425*, 497–502. [CrossRef] [PubMed]
8. Bown, D.P.; Gatehouse, J.A. Characterization of a digestive carboxypeptidase from the insect pest corn earworm (Helicoverpa armigera) with novel specificity towards C-terminal glutamate residues. *Eur. J. Biochem.* **2004**, *271*, 2000–2011. [CrossRef]
9. Edge, M.; Forder, C.; Hennam, J.; Lee, I.; Tonge, D.; Hardern, I.; Fitton, J.; Eckersley, K.; East, S.; Blakey, D.; et al. Engineered human carboxypeptidase B enzymes that hydrolyse hippuryl-L-glutamic acid: Reversed-polarity mutants. *Protein Eng.* **1998**, *11*, 1229–1234. [CrossRef]
10. Garcia-Guerrero, M.C.; Garcia-Pardo, J.; Berenguer, E.; Fernandez-Alvarez, R.; Barfi, G.B.; Lyons, P.J.; Aviles, F.X.; Huber, R.; Lorenzo, J.; Reverter, D. Crystal structure and mechanism of human carboxypeptidase O: Insights into its specific activity for acidic residues. *Proc. Natl. Acad. Sci. USA* **2018**, *115*, E3932–E3939. [CrossRef]
11. Teplyakov, A.; Polyakov, K.; Obmolova, G.; Strokopytov, B.; Kuranova, I.; Osterman, A.L.; Grishin, N.; Smulevitch, S.; Zagnitko, O.; Galperina, O.; et al. Crystal structure of carboxypeptidase T from *Thermoactinomyces vulgaris*. *Eur. J. Biochem.* **1992**, *208*, 281–288. [CrossRef]

12. Osterman, A.L.; Stepanov, V.M.; Rudenskaia, G.N.; Khodova, O.M.; Tsaplina, I.A. Carboxypeptidase T—intracellular carboxypeptidase of Thermoactinomycetes—A distant analog of animal carboxypeptidase. *Biokhimiia* **1984**, *49*, 292–301. [PubMed]

13. Grishin, A.M.; Akparov, V.K.; Chestukhina, G.G. Structural principles of the broad substrate specificity of *Thermoactinomyces vulgaris* carboxypeptidase T—Role of amino acid residues at positions 260 and 262. *Protein Eng. Des. Sel. Engl.* **2008**, *21*, 545–551. [CrossRef]

14. Akparov, V.K.; Grishin, A.M.; Yusupova, M.P.; Ivanova, N.M.; Chestukhina, G.G. Structural principles of the wide substrate specificity of *Thermoactinomyces vulgaris* carboxypeptidase T. Reconstruction of the carboxypeptidase B primary specificity pocket. *Biochemistry* **2007**, *72*, 416–423. [CrossRef]

15. Akparov, V.; Timofeev, V.; Khaliullin, I.; Švedas, V.; Kuranova, I.; Švedas, V. Structure of the carboxypeptidase B complex with N-sulfamoyl-L-phenylalanine—a transition state analog of non-specific substrate. *J. Biomol. Struct. Dyn. Engl.* **2018**, *36*, 956–965. [CrossRef] [PubMed]

16. Akparov, V.K.; Timofeev, V.I.; Konstantinova, G.E.; Khaliullin, I.G.; Kuranova, I.P.; Rakitina, T.V.; Švedas, V. The nature of the ligand's side chain interacting with the S1'-subsite of metallocarboxypeptidase T (from *Thermoactinomyces vulgaris*) determines the geometry of the tetrahedral transition complex. *PLoS ONE* **2019**, *14*, e0226636. [CrossRef] [PubMed]

17. Okai, M.; Yamamura, A.; Hayakawa, K.; Tsutsui, S.; Miyazono, K.I.; Lee, W.C.; Nagata, K.; Inoue, Y.; Tanokura, M. Insight into the transition between the open and closed conformations of Thermus thermophilus carboxypeptidase. *Biochem. Biophys Res. Commun.* **2017**, *484*, 787–793. [CrossRef]

18. Akparov, V.K.; Belianova, L.P.; Baratova, L.A.; Stepanov, V.M. Subtilisin 72: A serine protease from Bac. subtilis strain 72—An enzyme similar to subtilisin Carlsberg. *Biokhimiia* **1979**, *44*, 886–891.

19. Liublinskaia, L.A.; Iakushcheva, L.D.; Stepanov, V.M. The synthesis of the peptide substrates of the subtilisin and its analogs. *Bioorg. Khim.* **1977**, *3*, 273–279.

20. Voiushina, T.L.; Liublinskaia, L.A.; Timokhina, E.A.; Stepanov, V.M. Synthesis of p-nitroanilides of acylated peptides catalyzed by thermolysin. *Bioorg. Khim.* **1987**, *13*, 615–622.

21. Cueni, L.B.; Bazzone, T.J.; Riordan, J.F.; Vallee, B.L. Affinity chromatographic sorting of carboxypeptidase A and its chemically modified derivatives. *Anal. Biochem.* **1980**, *107*, 341–349. [CrossRef]

22. *Novagen pET System Manual TB055*, 7th ed.; Novagen: Madison, WI, USA, 1997.

23. Takahashi, S.; Tsurumura, T.; Aritake, K.; Furubayashi, N.; Sato, M.; Yamanaka, M.; Hirota, E.; Sano, S.; Kobayashi, T.; Tanaka, T.; et al. High-quality crystals of human haematopoietic prostaglandin D synthase with novel inhibitors. *Acta Cryst. Sect. F Struct. Biol. Cryst. Commun.* **2010**, *66*, 846–850. [CrossRef]

24. Garcia-Ruíz, J.M.; Gonzalez-Ramirez, A.L.; Gavira, J.A.; Otálora, F. Granada Crystallisation Box: A new device for protein crystallisation by counter-diffusion techniques. *Acta Crystallogr. Sect. D Biol. Crystallogr.* **2002**, *58*, 1638–1642. [CrossRef] [PubMed]

25. Takahashi, S.; Ohta, K.; Furubayashi, N.; Yan, B.; Koga, M.; Wada, Y.; Yamada, M.; Inaka, K.; Tanaka, H.; Miyoshi, H.; et al. JAXA protein crystallization in space: Ongoing improvements for growing high-quality crystals. *J. Synchrotron Radiat. Int. Union Crystallogr.* **2013**, *20*, 968–973. [CrossRef] [PubMed]

26. Takahashi, S.; Koga, M.; Yan, B.; Furubayashi, N.; Kamo, M.; Inaka, K.; Tanaka, H. JCB-SGT crystallization devices applicable to PCG experiments and their crystallization conditions. *Int. J. Microgravity Sci. Appl.* **2019**, *36*, 1–9.

27. McPherson, A. Macromolecular crystal growth in microgravity. *Crystallogr. Rev.* **1996**, *6*, 157–308. [CrossRef]

28. Battye, T.; Kontogiannis, L.; Johnson, O.; Powell, H. iMOSFLM: A new graphical interface for diffraction-image processing with MOSFLM. Leslie, AG. *Acta Crystallogr. D Biol. Crystallogr.* **2011**, *67 Pt 4*, 271–281. [CrossRef]

29. McCoy, A.J.; Grosse-Kunstleve, R.W.; Adams, P.D.; Winn, M.D.; Storoni, L.C.; Read, R.J. Phaser crystallographic software. *J. Appl. Crystallogr.* **2007**, *40*, 658–674. [CrossRef]

30. Murshudov, G.N.; Skubák, P.; Lebedev, A.A.; Pannu, N.S.; Steiner, R.A.; Nicholls, R.A.; Winn, M.D.; Long, F.; Vagin, A.A. REFMAC5 for the refinement of macromolecular crystal structures. *Acta Crystallogr. Sect. D Biol. Crystallogr.* **2011**, *67*, 355–367. [CrossRef] [PubMed]

31. Emsley, P.; Cowtan, K. Coot: Model-building tools for molecular graphics. *Acta Crystallogr. Sect. D Biol. Crystallogr.* **2004**, *60*, 2126–2132. [CrossRef]

32. Park, J.D.; Kim, D.H.; Kim, S.J.; Woo, J.R.; Ryu, S.E. Sulfamide-based inhibitors for carboxypeptidase A. Novel type transition state analogue inhibitors for zinc proteases. *J. Med. Chem.* **2002**, *45*, 5295–5302. [CrossRef] [PubMed]